2.0 Summary

This chapter deals with the experimental techniques used in preparation, characterization and analysis of the permalloy samples. The design of hydrogen annealing furnace, die and punch and other necessary experimental set-up is described. The method of measurement of magnetic properties is also explained.

2.1 Sample preparation

The raw materials used for the experiments were commercially available FeO, NiO etc. Many techniques have been reported for the preparation of high purity metals, however, we have chosen the vacuum –melting technique because it is effective and suitable for Fe, Co and Ni systems [1-3]. Melting of a metal in vacuum serves two special purposes. It removes the normal atmosphere surrounding the metal, so that there will be no possibility for the molten metal to be contaminated by oxygen and nitrogen. It also removes certain impurities from the metal through one of processes like dissociation, deoxidation and degassing. The effectiveness of the vacuum –melting technique in removing the gaseous elements (O, N, H) and sulfur is shown in Table 2.1 [4]. Typical contents of these impurities before and after vacuum induction melting in iron, cobalt and nickel are compared.

The set-up required for the vacuum melting essentially consists of a vacuum chamber for housing the crucible, a pumping system and necessary melting facilities for the pouring mechanism. The pumping system should be capable of pumping down the chamber to 10^{-3} torr or less during the melting. The crucible used for melting Fe, Co, Ni alloys is made up of alumina. Melting of the alloys in vacuum is best effected by induction heating, because of electromagnetic force set up in the molten metal produces a stirring action. This stirring action continuously expose new surfaces of the molten metal to the action of pumping, thus promoting the degassing process. Also, it helps in homogenizing the liquid mixture when the alloy is being prepared. The selection of frequency of the alternating current is also important. Lower frequencies provide not only deeper penetration but also vigorous stirring. Frequencies upto 10 KHz are useful in vacuum induction melting and can be obtained conveniently from motor generator.

Table 2.1: Typical contents of iron, cobalt and nickel before and after vacuum- induction melting

	Impurity Content (wt. ppm)			
Metal	Oxygen	Nitrogen	Hydrogen	Sulfur
Before vacuum-induction melting				
Iron (ingot)	900	10	≤10	150
Iron (electrolytic)	100	100	100	50
Cobalt (electrolytic)	70	10	8	--
Nickel (carbonyl)	30	10	≤100	--
Nickel (270)	≤100	≤100	≤100	--
After vacuum-induction melting				
Iron	20	2	-	30
Cobalt	50	-	-	30
Nickel	10	1	-	30

The samples prepared by vacuum induction melting were hot pressed to slabs and then hot and cold rolled to 0.30 to 0.60 mm thick strip. The cold rolled strip was slit to 35 mm width for core production.

2.2 Nickel-iron phase diagram

The equilibrium phase diagram for binary nickel-iron alloys is shown in Fig. 2.1 [5]. When the alloys from 30 to 100% Ni were cooled from high temperature to room temperature, the face centered cubic (fcc) γ phase exists in these alloys. The importance of the alloys is the appearance of the long-range ordered Ll_2 structure at the Ni_3Fe composition below 500 ± 5°C. The ordered kinetics is very slow and takes at least one-week time to reach maximum value of order. Above the order-disorder temperature, the alloys in the vicinity of Ni_3Fe composition exhibit short-range order, the kinetics of

which is rather fast. This is due to the large change in the value of the magnetocrystalline anisotropy energy (K_1). Therefore, the variations in isothermal treatment temperature and cooling rates have a drastic effect on the magnetic properties such as permeability [6]. Doping of alloying elements such as Mo, Cr and Cu tend to slow down the ordering kinetics and lowers the degree of long range order, while additives such as Mn and Si tend to stabilize it [7-8]. Fig. 2.2 shows the variation of the long range order parameter S with alloy content for alloys of approximately Ni / Fe = 3/1 composition [6]. Actually, Mo and Cr replace Fe atoms and strongly bond with Ni, causing destruction of Ni_3Fe super lattice whereas Mn bonds lightly with Ni and has no influence on Ni_3Fe order. Also, Cu, Co and Si replace Ni atoms. The first two bond strongly with Fe and perturbs Ni_3Fe order, while the latter bond lightly, causing no perturbation. The creation of short-range order with predominant MoNi and CrNi bonds in these ternaries is mainly responsible for the rise in electrical resistivity [7-10]. The creation of long-range order in Ni_3Fe results in the decrease in resistivity.

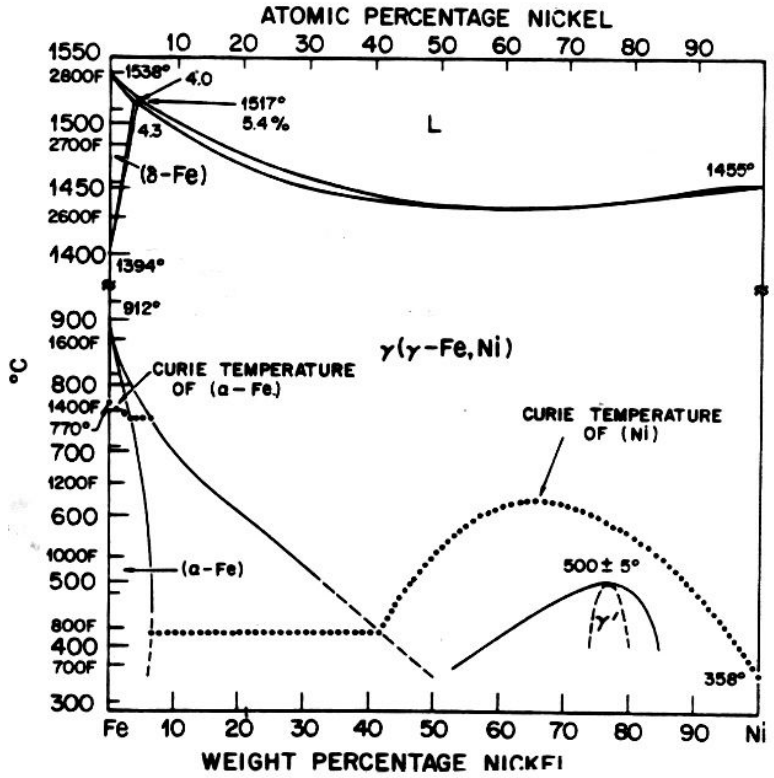

Fig. 2.1: A typical Ni-Fe phase diagram [5]

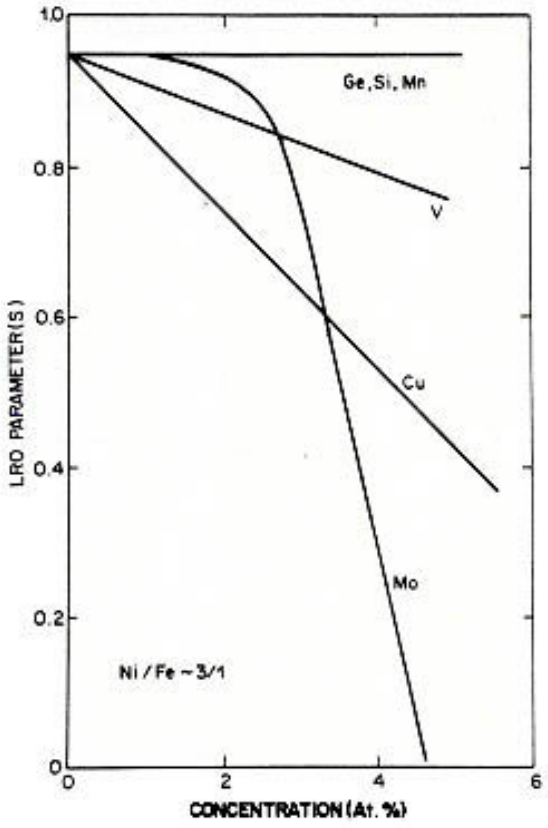

Fig. 2.2: Variation of long range parameter with alloy content

2.3 Chemical composition of samples

Chemical composition of the soft magnetic alloys is very important because small amounts of impurities drastically affect the magnetic properties of the alloys. The elements and composition of the samples were determined by wet chemical analysis and atomic absorption spectrometer [11]. Atomic absorption spectrometer (GBC, Model 932 AA) offers a minimum detection limit ranging from few parts per million (ppm) to parts per billion (ppb) and can analyse trace impurities in almost all the elements and alloys. The composition of samples A, B and C are given in the Table 2.2.

Table 2.2: Chemical compositions of the permalloy samples studied in this work

Element	Sample A	Sample B	Sample C
Ni	82.13	79.90	47.01
Fe	12.38	14.47	49.50
Mo	4.90	5.00	-
Mn	0.41	0.43	0.38
C	0.01	0.02	0.05
Si	0.10	Traces	0.63
Cr	0.10	-	-
Co	0.05	-	0.03
Cu	0.05	-	-

2.4 Punching of ring samples

The die and punch was indigenously designed and fabricated from high speed steel having hardness of 55-60 HRc. The drawings of the die and punch are given in Fig. 2.3. The rings of size, outer diameter = 10 mm and inter diameter = 6 mm were made from the die and punch assembly (shown in Fig. 2.4). This technique was also used for punching audio head and watch components. The details are given in chapter 5.

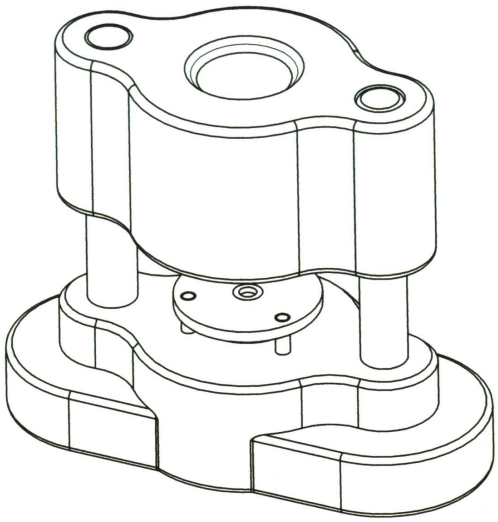

Fig. 2.3a: Schematic view of the die

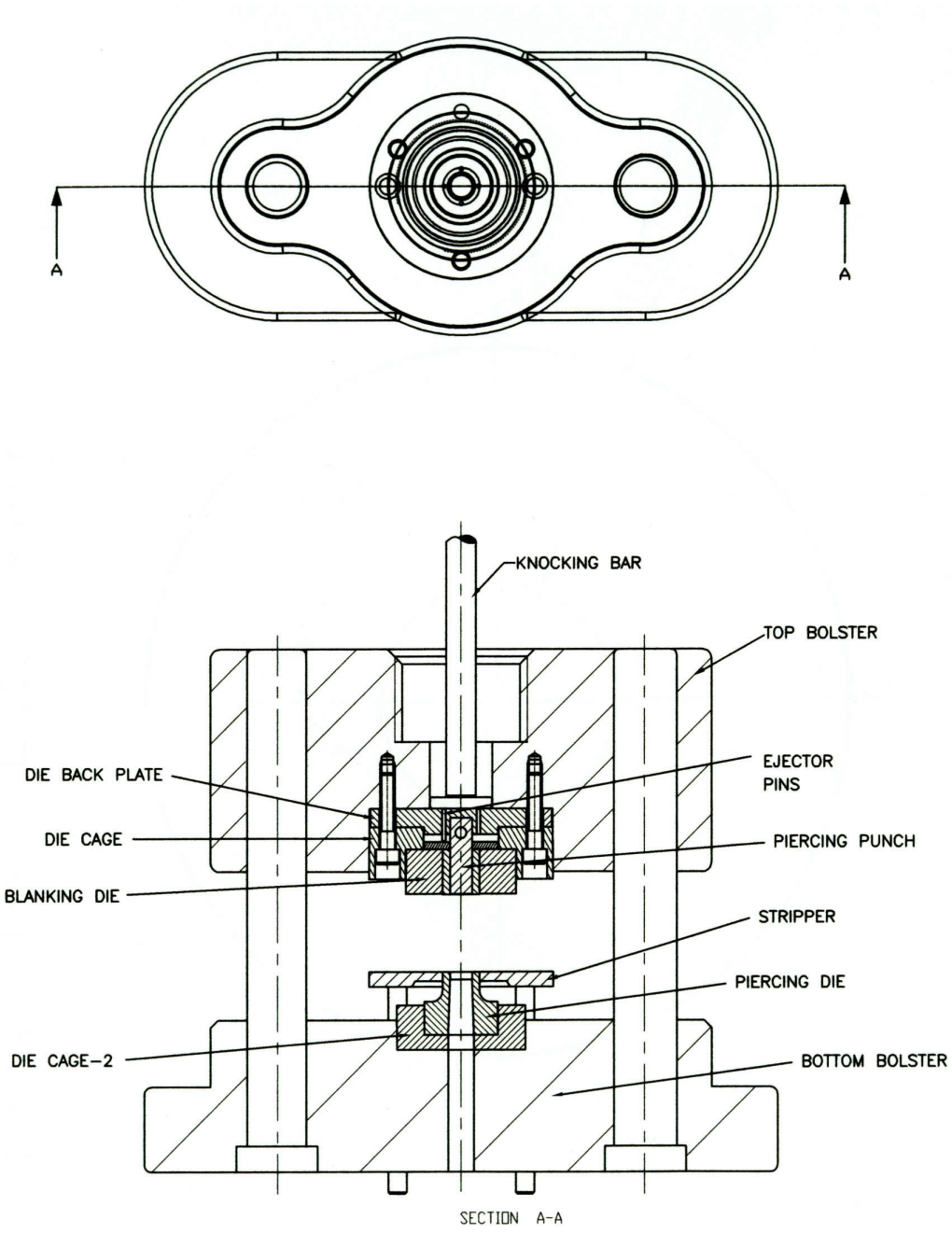

Fig. 2.3b: Sectional view of the die

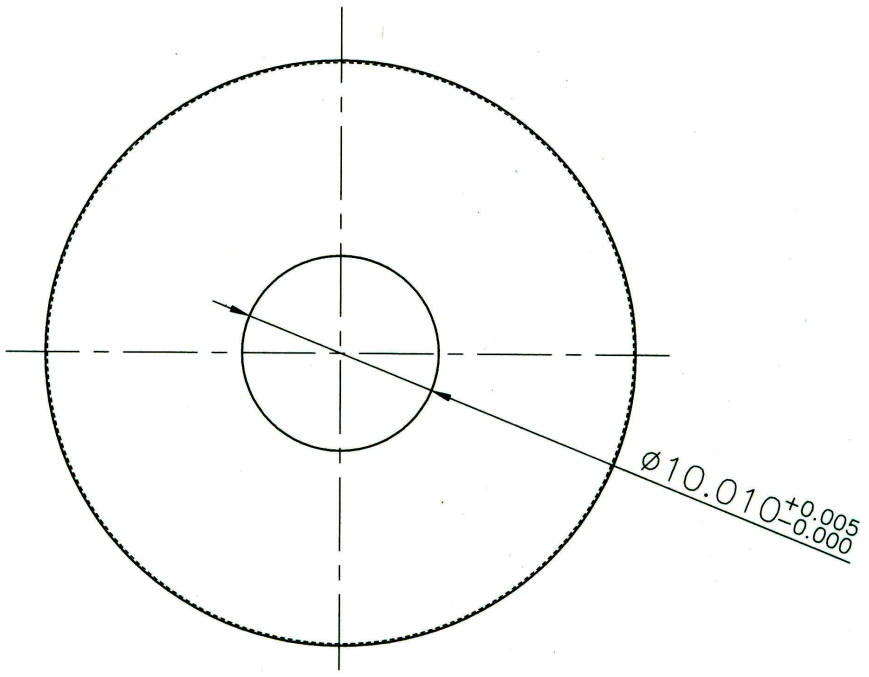

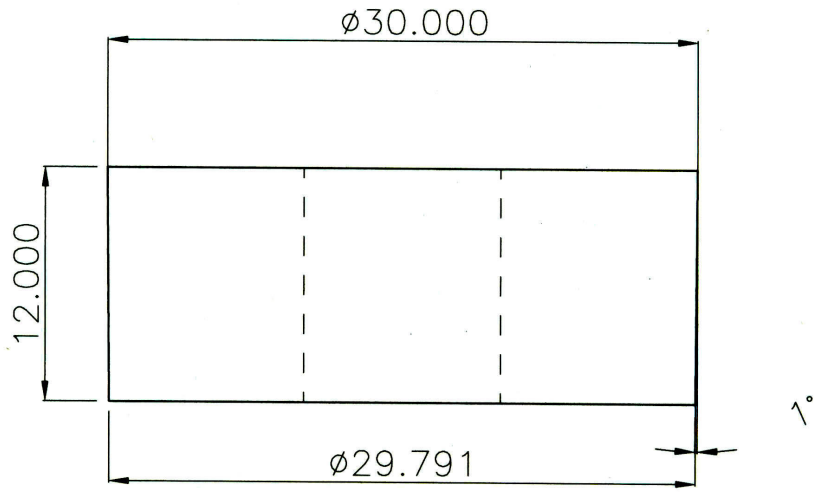

All dimensions are in mm.

Fig. 2.3c: Drawing of the blanking die

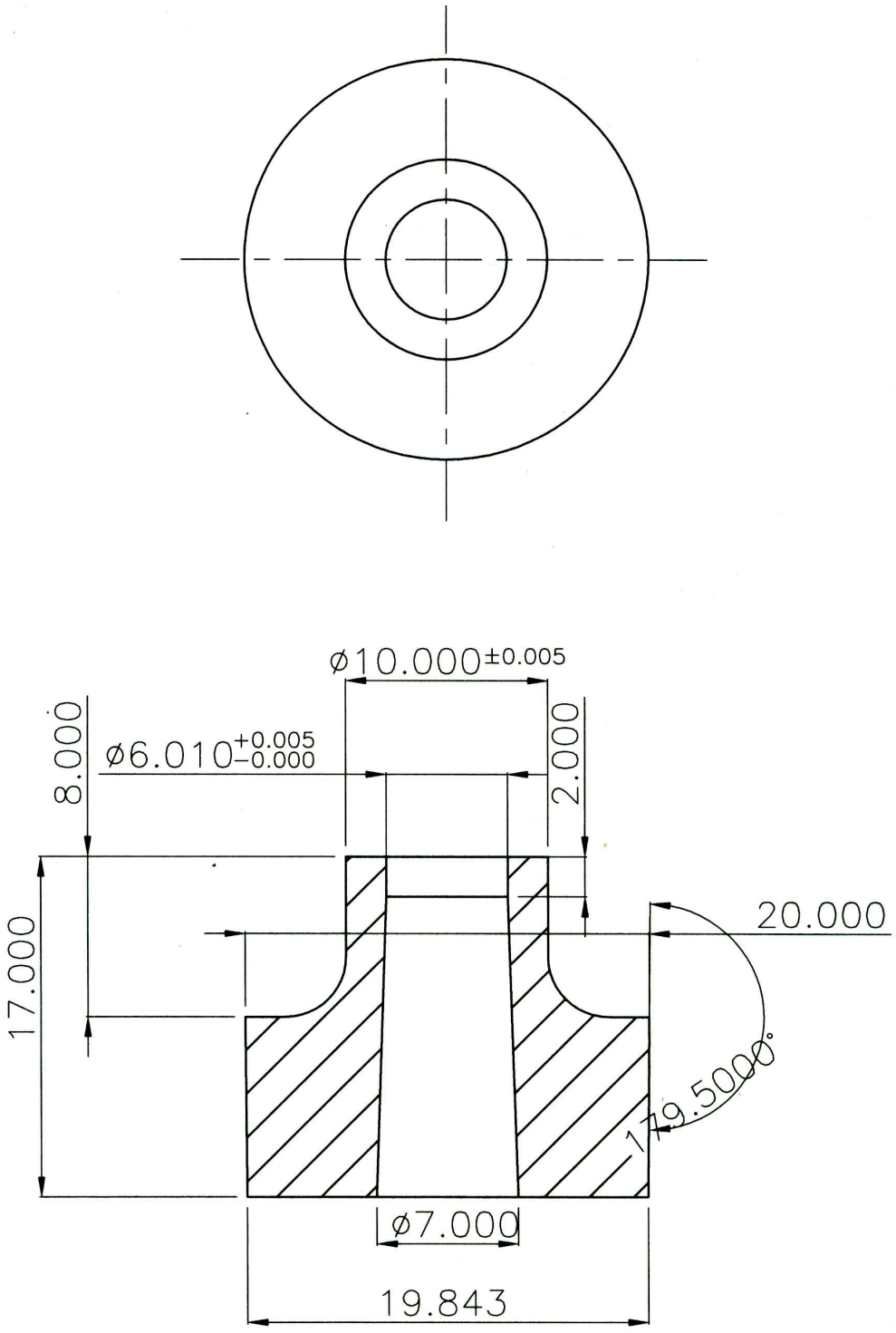

All dimensions are in mm.

Fig. 2.3d: Drawing of the piercing die

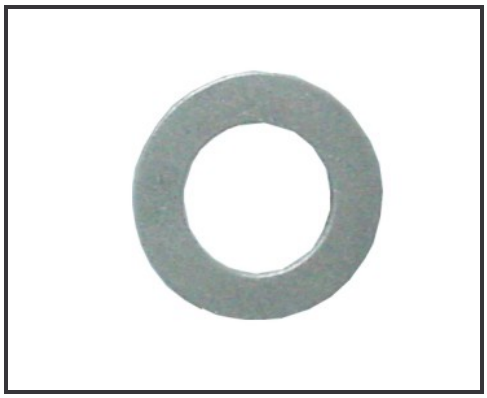

Fig. 2.4: Photograph showing permalloy sample in a ring shape

2.5 Annealing and recrystallization

The manufacturing methods of magnetic materials generate stresses and introduce impurities like carbon, oxygen and sulphur in the materials. These impurities are especially deleterious to ferromagnetic properties because they distort the crystal structure lattice and even in small amounts may greatly interfere with easy movement of magnetic domains, which is the basis of such properties [12]. Each of these factors contributes to the degradation of performance of magnetic materials. The processing of soft magnetic materials involves a special heat treatment called annealing in H_2 atmosphere to restore its magnetic properties. The magnetic properties of the materials depend on the annealing temperature and cooling rate. Annealing improves the properties of materials by relieving cold work stresses and by recrystallising the grain structure. The cooling rate helps to restore the magnetic properties [6, 13-14]. To improve the properties, a protective atmosphere was used during heating to prevent any damage to the materials. For this, suitable atmosphere is high purity dry hydrogen gas with a dew point below -40°C [15]. Dry hydrogen removes carbon, oxygen and sulfur from the alloy, making it a bright, clean surface.

Annealing is a heat treatment in which a material is exposed to an elevated temperature (about 50% of the absolute melting temperature) for an extended time period and then slowly cooled in order to give them the desired microstructure and magnetic properties.

The time - temperature cycle and atmosphere composition are critical process parameters. Bright annealing always required reducing atmosphere in order to avoid oxidation and to produce a bright, clean surface [6]. Usually nitrogen or nitrogen/hydrogen atmosphere is recommended. The annealing process can be divided into three fairly distinct groups: recovery, recrystallization and grain growth, which are associated with the annealing of a plastically deformed crystalline material [16-17].

2.5.1 Design and development of heat treatment furnace

A muffle furnace was designed and developed in our laboratory. The working capacity of the furnace was ½Kg for material processing upto 1200°C temperature [18]. The furnace was controlled by the dedicated temperature profile controller with a interface to phase controlled power supply. The block diagram of the experimental set-up is shown in Fig. 2.5. The system consists of voltage stabilizer (3KW), uninterrupted power supply (UPS), thyristor power pack, temperature profiler/controller, muffle furnace, R-type thermocouple, binary gas analyzer, arrangements for purging H_2 and N_2 gas in the furnace and burning of H_2 gas.

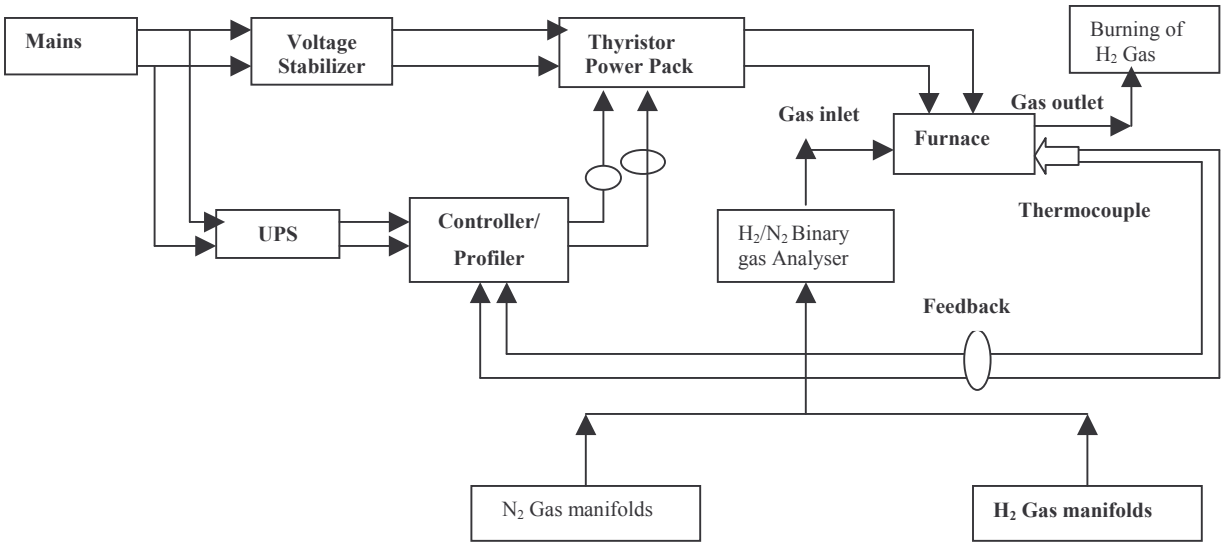

Fig. 2.5: Block diagram of the experimental set-up

The schematic diagram of the muffle furnace and its assembly is given in Fig 2.6 and Fig. 2.7 respectively. The muffle selected for the furnace was made up of high alumina of length 1000 mm and outer diameter of 60mm. Four number of silicon carbide heating elements connected in series have been used for heating the muffle from outside to reach the desired temperature inside the muffle. The total wattage of the furnace was 3KW. The radiation shielding was provided outside the heaters to attain better heat efficiency towards the muffle. The ceramic muffle was insulated with zirconia wool and its both ends were closed with stainless steel blocks designed precisely to make the muffle totally gas leak proof. These blocks were joined with the muffle using temperature sealant. The water circulation on the SS blocks was provided by making it double jacket to protect from over heating of the temperature sealant. The outer bodies of the furnace were made up of stainless steel and mild steel respectively. The heating and cooling of the furnace were controlled by temperature profile controller and thyristor power pack. A uniform heating zone of 180mm (lengthwise in center) was attained inside the furnace. The arrangements for the H_2 atmosphere inside the furnace chamber were made with the help of copper pipe. In the outlet, H_2 gas was kept burning throughout the annealing process.

Control of the furnace

Temperature profiler/controller (N 6400, West Instruments) was used to control the heating rate, cooling rate and holding time of the furnace. Temperature versus time graph and output of the thermocouple was fed to the controller. A built-in amplifier in the controller amplifies the weak signal of milli volt range and converts it into a strong signal in voltage range. This signal was read by the controller in terms of corresponding temperature. It has a built-in PID controller which senses the actual temperature of the furnace, compares it with the set temperature versus time curve and accordingly, generates a 4-20mA control output. This output was further fed to the thyristor power pack.

A thyristor power pack (CD 2300, Toshniwal, Ajmer) is a phase controlled power supply. It accepts 4-20 mA control signal from the temperature controller and sets up the corresponding output AC voltage (0-230 V) to the heaters. Therefore, the input power of the heaters was controlled. A thyristor power pack of 40A current rating was selected.

Binary gas analyzer (4235 PB, Nucon Engineers, New Delhi) was used to monitor the gas environment inside the furnace chamber.

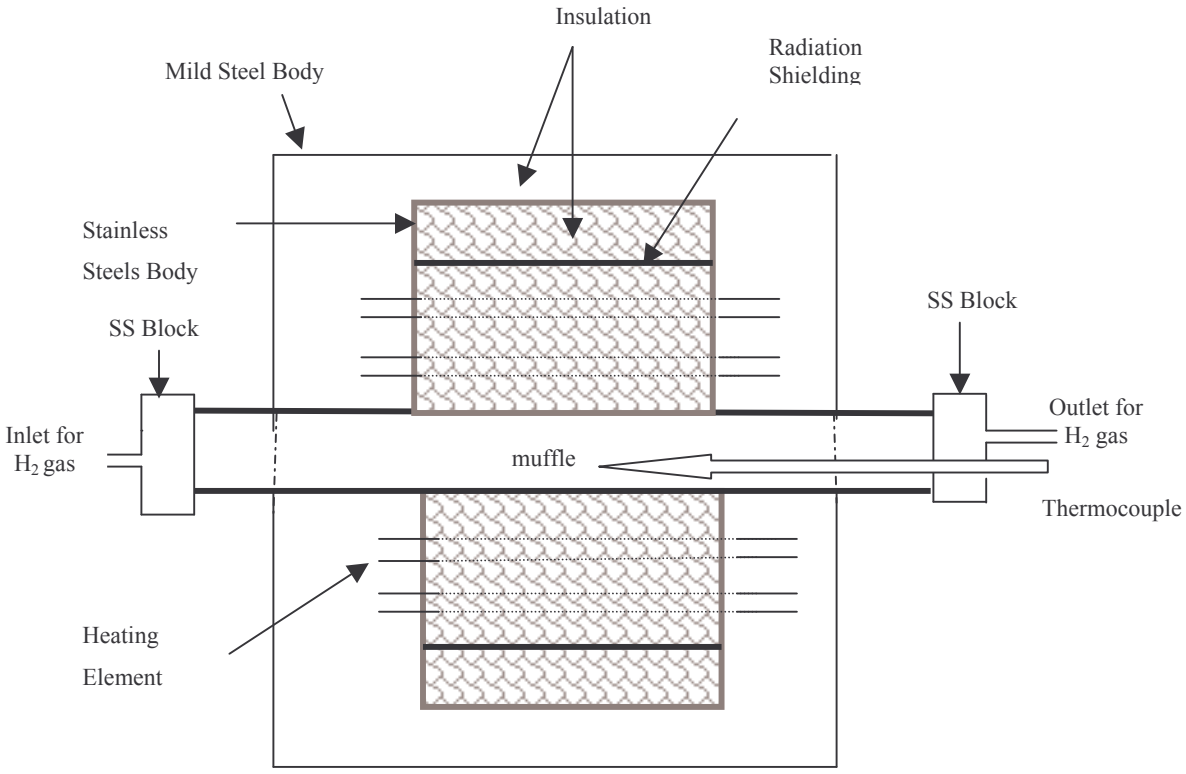

Fig. 2.6: Schematic diagram of hydrogen annealing muffle furnace

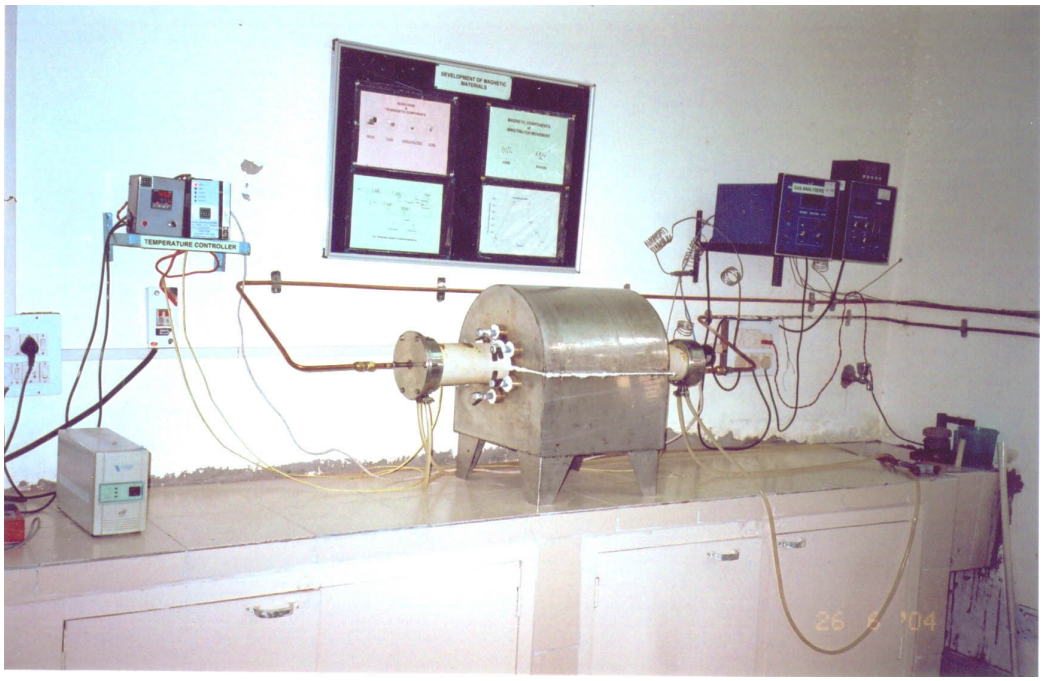

Fig. 2.7: Assembly of the annealing furnace

Calibration of the furnace

The calibration of the muffle furnace was carried out for its temperature sensor unit (i.e. R-type thermocouple with temperature indicator) with the standard thermocouple (calibrated by NPL, New Delhi). The uniform temperature with ± 2°C at 1200°C was achieved in the muffle furnace.

2.5.2 Annealing profiles

The unwanted contaminants like oil, grease etc. were removed from the samples using soap solution before annealing. The individual parts of the samples were separated by an inert insulating powder such as aluminum oxide during hydrogen annealing. The ring samples were annealed in H_2 atmosphere in the temperature range of 1100-1180°C under different processing parameters like variable holding time, cooling rate and annealing temperature. The different annealing profiles performed on the samples are given in the Table 2.3.

Table 2.3: Annealing Profiles performed on the samples

Annealing Temperature (°C)	**Holding Time (h)**	**Cooling rate through the ordering range (700-300°C) (°C/min)**
1100, 1120, 1140, 1150, 1160, 1180	2	2.5
1150	1, 2, 3	2.5
1150	2	2.0, 2.5, 3.0, 5.0, 7.0

2.6 XRD analysis

X-Ray Diffraction (XRD) technique is used to identify the phases present in samples from raw starting materials to finished products and to provide information on the physical state of the sample, such as grain size, texture and crystal perfection. The X-ray diffraction technique is rapid and non-destructive.

X-rays are generated when any electrically charged particle with sufficient kinetic energy rapidly decelerates. When an x-ray beam impinges a metal an interesting interaction (known as Thompson scattering) occurs. This interaction causes the electrons to emit electromagnetic radiation of the same wavelength, λ, as the impinged beam, and this produces a diffraction effect. A beam of radiation of wavelength λ hits the crystal at some θ angle. The diffraction will produce a strong reflection from the crystal at an angle α only if the following conditions are all met:

1. Only one α angle is possible, $\alpha = \theta$
2. The Bragg law must be satisfied.

$$n\lambda = 2\, d_{hkl} \,.\, \sin\theta \qquad (2.1)$$

where n is an integer number, λ is the radiation wavelength, d_{hkl} is the distance between planes and θ is the x-ray's angle of incidence. For the cubic crystals the lattice constant can be calculated using equation 2.2 [16].

$$d_{hkl} = \frac{a}{\sqrt{h^2 + K^2 + l^2}} \qquad (2.2)$$

The phase analysis of the annealed samples was carried out by X-ray Diffractometer (Rigaku, D-max IIIC) as shown in Fig. 2.8. The diffractometer comprised of a copper target, a curved single crystal monocromator of graphite and NaI scintillation counter as a detector. The strip sample used for analysis was of the size (19 mm X 17mm) held in 0.5 mm deep cavity of a sample holder with the help of binder. Diffraction pattern was recorded at a scanning speed of 3° per minute. The sample data was matched with the standard database compiled in software PCPDFWIN provided by the International Centre for Diffraction Data –ICDD (formely known as JCPDS-The joint Committee on Powder Diffraction Standards) [19-20]. The software is a compilation of a single phase X-ray powder diffraction patterns in the form of tables of characteristic inter planer spacing and corresponding relative intensities along with other pertinent physical and crystallographic properties.

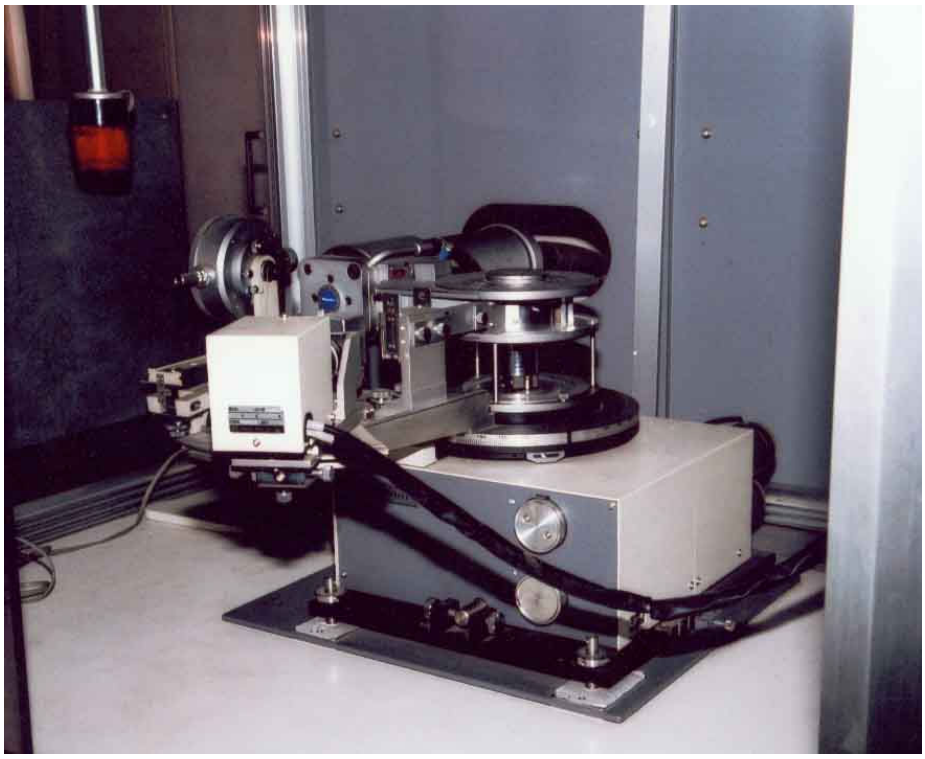

Fig. 2.8: X-ray diffractograph

2.7 Microstructural analysis

One of the foundations of modern materials science is the acknowledgment of the fact that the properties and performance of materials are intrinsically related to their microstructure [21]. Microstructural analysis is the combined characterization of the morphology, elemental composition and crystallography of microstructural features through the use of a microscope. Light microscopes have been used to characterize the microstructures of metals for over 100 years.

2.7.1 Metallographic sample preparation

Mechanical polishing

For the mechanical polishing the specimens were hot mounted in a Bakelite powder at 110°C using mounting press (Madras Metallurgical Services Pvt. Ltd., Hyderabad). The polishing procedure involved initial grinding using silicon carbide paper of 400, 600 and 1000 grit with 45 to 90° rotation of specimen between grinding steps followed by rough polishing using 3 micron and 1micron diamond paste on low-nap cloth at a speed of 350 rpm for 15 minutes. The machine used for both grinding and polishing was made up of Buehler, USA. An oxide polishing, using a solution of Al_2O_3 and distillated water was also performed on all samples to eliminate any deformed or stressed layer formed during the grinding and polishing operations.

Etching

Etching was performed using a mixture of 50 ml HCl, 10 g $CuSO_4$ (copper sulphate), 50 ml H_2O [22]. This is also known as Marble's reagent.

2.7.2 Optical microscopy

After the proper polishing and etching, the microstructural analysis was carried out using optical microscope (Nikon, Japan) for. Several micrographs were taken in order to precisely evaluate the microstructure of each sample using image analysis system (Sis, Germany) [Please see Fig. 2.9]. The average grain size of the samples was evaluated using the linear intercept method [23]. Equation 2.3 represents the linear intercept

method, where d is the diameter of the grain, L is the length of the line, N is the number of intersections and M is the image's magnification.

$$d = \frac{L}{NM} \tag{2.3}$$

Fig. 2.9: Image analysis system

2.8 Magnetic measurements

Properly prepared ring samples and toroids provide the most accurate method for measuring the magnetic properties of soft magnetic material [24]. The toroid shape samples were prepared by stacking rings having outer and inner diameter of 10mm and 6mm and using 20 numbers of primary and secondary turns. AC magnetic measurements under different processing parameters were carried out using B-H Analyser (AMH-401, Walker Scientific, USA). The magnetic measurement set-up and its block diagram are given in Fig. 2.10 and Fig. 2.11 respectively.

The AMH-401 is a PC based hysteresisgraph for measuring the magnetic properties of soft materials at frequencies from 50 Hz to 100 kHz with its own built-in power

amplifier. Both core loss and hysteresis loop parameters (with curves) are displayed on a high resolution color monitor. It provides accuracy of ± 2 % for B or H values and ± 5 % for core loss [25].

Fig. 2.10: Magnetic measurement set-up

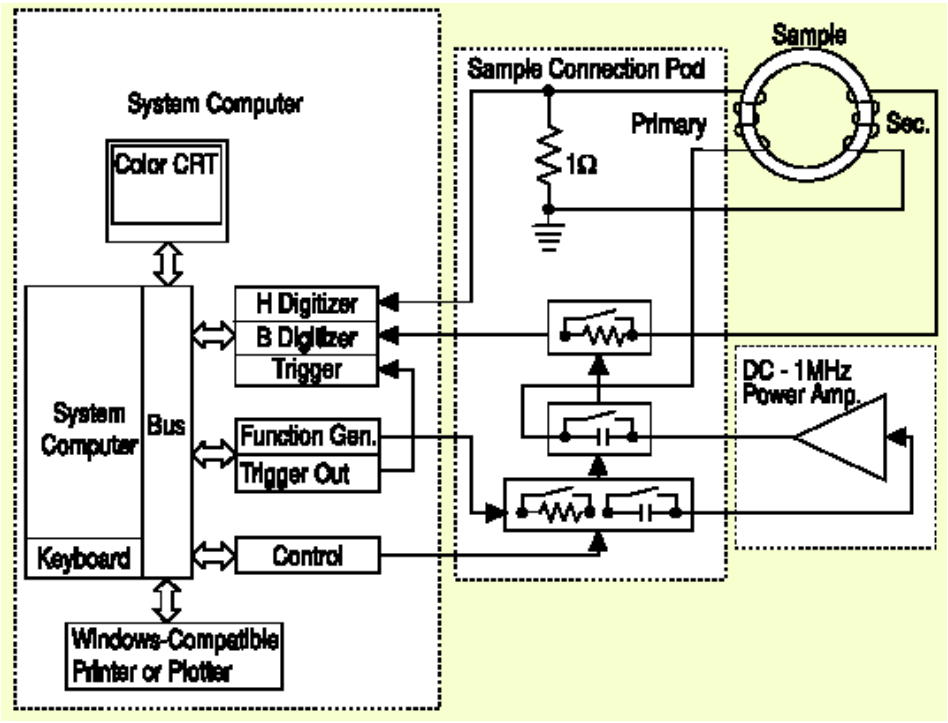

Fig. 2.11: Block diagram of AMH-401

References

1. C. W. Chen, Magnetism and Metallurgy of Soft Magnetic Materials, North Holland Publishing Company, 1977
2. Lin Li, IEEE Trans. Magn., **37** (2001) 2315
3. Lin Li & M. S. Masteller, IEEE Trans. Magn., **33** (1997) 3769
4. W. F. Mooree, Techniques of materials preparation and handling, Bunsah, R. F. ed. (Interscience Publishers, New York) **1part 2** (1968)
5. J. I. Goldstein, Metals Hand Book (Am. Soc. Met., Metals Park, OH), **8** (1973) 304
6. G. Y. Chin & J. H. Wernick, Ferromagnetic materials, A handbook on the properties of magnetically ordered substances edited by E P Wohlfarth, (North Holland Publishing Co.), **2** (1980)
7. V. I. Goman'kov, I. M. Puzei, A. A. Loshmanov & Ye. I. Mal'tzev, Phys. Met. Metallogr., **28** (1969) 77
8. V. I. Goman'kov, I. M. Puzei & Ye. I. Mal'tzev, Phys. Met. Metallogr., **30** (1970) 237
9. H. Thomas, Z. Phys., **129** (1951) 219
10. F. Pfeifer & I. Pfeiffer, Z. Metallk., **55** (1964) 398
11. ASM Hand Book, Desk edition, ASM International, USA, 1998
12. R. D. Enoch & A. D. Fudge, Brit. J. Appl. Phys., **17** (1966) 623
13. G. Y. Chin, IEEE Trans. Magn. **7** (1971) 102
14. F. Pfeifer, Encyclo. Mater. Sci. & Engg., **4 (**1986) 2663
15. F. Pfeifer & C. Radeloff, J. Magn. Magn. Mater., **19** (1980) 190
16. V. Raghavan, Materials Science and Engineering- A First Course, 1995
17. R. D. Doherty, D. A. Hughes, F. J. Humphreys, J. J. Jonas, D.J. Jensen, M.E. Kassner, W.E. King, T.R. McNelley, H.J. McQueen & A.D. Rollett, Mater. Sci. Engg., **A238** (1997) 219
18. Project report, Development & characterization of magnetic materials & components for audio recording applications, NRTC, 2002
19. JCPDS-International Centre for Diffraction Data, PCPDFWIN, **2.02** (1999)
20. B. D. Cullity, Elements of X-ray diffraction, 3rd ed., Prentice –Hall, Upper Saddle River, N J, 2001

21. K. J. Kurzydlowski & B. Ralph, The Quantitative Description of the Microstructure of Materials, CRC Press, New York, 1995
22. ASM Handbook of Metallography and Microstructures, ASM Internationals, USA, **9 (**1985)
23. Indian Standard : Methods for estimating average grain size of metals, 4748 (1988)
24. H. Zijlstra, Experimental Methods in Magnetism, North Holland Publishing Co., Amsterdam, (1967)
25. Instruction Manuals, Automatic Hysteresisgraph, AMH-401, Walker Scientific Inc., USA, 1997